Lab on a Chip

TECHNICAL INNOVATION

Fabrication of polydimethylsiloxane (PDMS) nanofluidic chips with controllable channel size and spacing †

Received 00th January 20xx,
Accepted 00th January 20xx

DOI: 10.1039/x0xx00000x

www.rsc.org/

Ran Peng, and Dongqing Li*

The ability of making reproducible and inexpensive nanofluidic chips is essential to the fundamental research and the applications of nanofluidics. This paper presents a novel and cost-effective method for fabricating a single nanochannel or multiple-nanochannels in PDMS chips with controllable channel size and spacing. Single nanocracks or nanocrack arrays, positioned by artificial defects, are first generated on a polystyrene surface with controllable sizes and spacing by solvent-induced method. Two sets of optimal working parameters are developed to replicate the nanocracks onto polymer layers to form the nanochannel molds. The nanochannel molds are used to make the bi-layer PDMS microchannel-nanochannel chips by simple soft lithography. An alignment system is developed for bonding the nanofluidic chips under an optical microscope. Using this method, high quality PDMS nanofluidic chips with a single nanochannel or multiple nanochannels of sub-100 nm in width and height and centimeters in length can be obtained with high repeatability.

1. Introduction

Nanochannel devices with structure size smaller than 100 nm are critical in experimental studies and applications of nanofluidics. Such a small size gives rise to many new transport phenomena in nanoscale due to the overlap of electric double layers (EDL) [1–4] and leads to possibilities of detection, manipulation and controlling of individual nanoscale targets, such as virus [5–7], bacteria [8,9], DNAs [10–15], proteins [16,17] and nanoparticles [14,18–20]. Therefore, relatively simple and reliable methods of fabricating small nanochannels are essential to these studies and applications.

Many techniques, from conventional to unconventional methods, and from up-down to bottom-up strategies, have been developed in fabricating of nanofluidic devices. These nanofabrication techniques have been reviewed by Duan et al. [21–24] Conventional photolithography [25] is a prevailing method in micropattern fabrication; however, this method is limited by the incident light and resolution of photomasks [25]. Deep UV [26] and x-ray [27,28] have been used to improve the resolution by reducing the wavelength of the incident light, however, the systems are complicated and the photomasks are expensive. Interferometric lithography (IL) [29], also referred to as interference lithography, is a powerful technique for fabricating simple periodical nanometer-sized structures over a large area, but it is not applicable for single nanochannels. Electron beam lithography (EBL) [30] and focused ion beam (FIB) lithography [31,32] are excellent tools for nanofabrication, however, these techniques are expensive and require professional training. Nanomaterials such as nanowires [33–36], nanotubes [37] and nanofibers [38] are also used in nano-device fabrication. However, the problems here are the difficulty to handle the tiny samples by mechanical tools and the difficulty to finalize the alignment during device assembling. Collapse of channel roofs [39], tunable elastomeric nanochannels [40,41] based on deformation of PDMS microchannels are novel strategies to create cost-effective nanochannel devices; however, these methods can hardly produce repeatable results.

Fabrication of crack-based nanochannels on polymer surfaces coined by Zhu et al [14,42,43] is a promising strategy with the merits of low cost and high productivity. Nanocrack arrays of centimetre long and 20 nm to 200 nm deep creating on polystyrene (PS) surfaces by using solvent-induced method was reported by Xu et al [44]. Afterwards, cracking on polystyrene surfaces by using the solvent-induced method has been systematically studied by Peng and Li [45], and a guideline for fabricating nanocracks with controllable size smaller than 100 nm was provided. However, the locations of the nanocracks and the spacing between the cracks are random. Consequently, it is difficult to fabricate one single nanochannel from these nanocracks and connect such a single nanochannel to microchannels to form a single nanochannel device, which is the core requirement for the fundamental studies of transport phenomena and manipulation of individual targets in nanoscale. In addition, in order to obtain accurate, repeatable and durable nanochannel molds, replication of nanocracks from polystyrene surfaces without changing the crack size is still a challenge. Furthermore, nanostructures duplicated by using regular PDMS are likely to collapse after bonding due to the low Young's modulus of the regular PDMS material.

*Department of Mechanical and Mechatronics Engineering,University of Waterloo, Waterloo, Ontario, Canada N2L 3G. *E-mail: dongqing@uwaterloo.ca*
Electronic Supplementary information (ESI) available

This paper presents a novel approach to fabricating a sealed single nanochannel or a sealed nanochannel array on PDMS chips. Single nanocracks or nanocrack arrays with controllable sizes and locations are generated on polystyrene surfaces by the solvent-induced method. These nanocracks are replicated onto SU-8 photoresist or smooth cast material to work as the nanochannel molds. Thereafter, these molds are used to produce the bi-layer PDMS nanochannels. Stable nanofluidic chips with high reproducibility are eventually obtained by bonding the PDMS nanochannel with a PDMS microchannel chip by using a homemade alignment system. Practical applications of these nanofluidic devices such as manipulation of individual nanoparticles, electric current properties in nanochannels have also been demonstrated in this paper.

2. Experimental details

2.1 Fabrication of single nanocracks and nanocrack arrays

Creating of nanocracks on polystyrene surfaces with controllable sizes and spacing is conducted by two steps. The first step is to make diamond-shaped artificial defects on polystyrene surfaces (petri dish surfaces (VWR®)) by using a micro-hardness testing indenter (LECO®, MHT series 200) (see Figure 1(a1)). The sizes and locations of the defects are controlled by the micro-hardness testing system. These defects promise the locations of the nanocracks.

Thereafter, nanocracks are generated from the defects by the solvent-induced method [45]. Briefly, a polystyrene slab with artificial defects is covered onto the open mouth (0.5 cm wide and 1 cm long) of a plastic reservoir filled with a chemical reagent such as ethanol. The reservoir is placed on a heat plate (Torrey Pines Scientific®) with precisely controlled heating temperature, as shown in Figure 1(a2). Consequently, the chemical reagent will vaporize and condense onto the inner surface of the polystyrene slab. The polystyrene surface will absorb the reagent and swell until the reagent is fully vaporized (Figure 1(a3)). Afterwards, the swelling layer will shrink and generate nanocracks due to the releasing of the absorbed reagent, as shown in Figure 1(a4). The crack size is adjustable according to the working parameters used in the solvent-induced method, such as concentration and volume of the reagent, heating temperature, heating time and so on [45].

2.2 Fabrication of nanochannel molds

Nanocracks on polystyrene surfaces are not stable and the crack size changes with time, temperature and chemical environment due to residual stress in the swelling layers. Furthermore, it is also time-consuming to repeat the solvent-induced cracking process. To fix the nanocrack size and to make reliable nanofluidic chips with high reproducibility, the negative nanocracks are replicated onto either SU8 photoresist (MicroChem Corp.) or Smooth cast 305 (Sculpture Supply Canada) by soft lithography method (method A in Figure 1) and nanoimprint technique (method B in Figure 1), respectively. Figure 1(b~d) shows the working principles of both method A and method B.

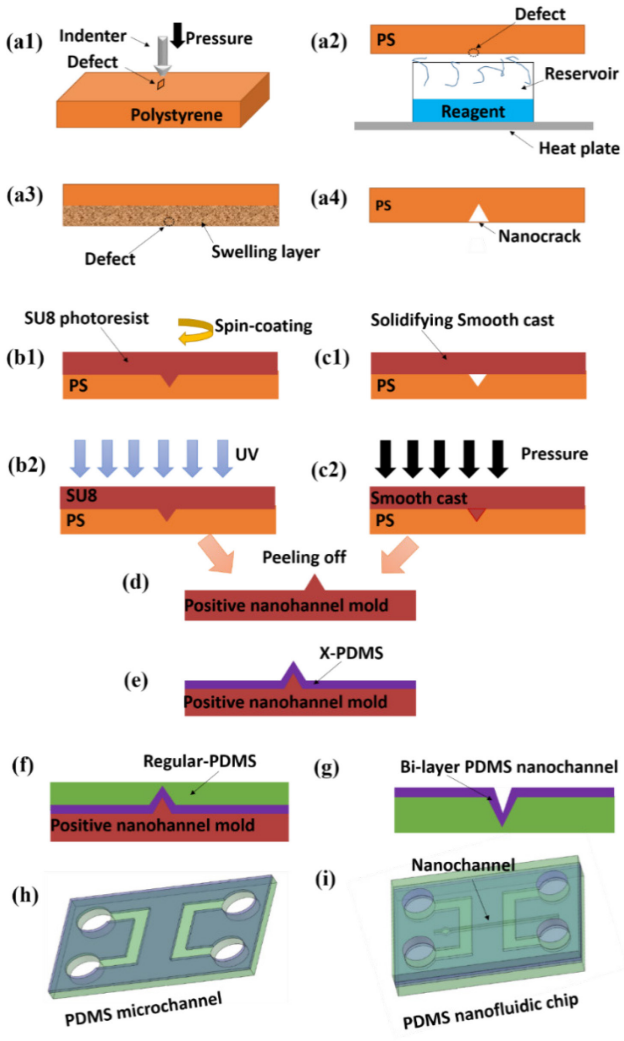

Figure 1 Working procedures for fabricating single or multiple nanochannels in a PDMS chip.

In method A, SU8 photoresist is spin-coated onto a polystyrene surface with a single nanocrack or a nanocrack array at a given speed for a given period of time by a spin-coater (Brewer Science Inc. Cee® 200X) (Figure 1(b1)) followed by exposure to UV light for a certain period of time (Figure 1(b2)). A stable SU8 photoresist nanochannel mold (Figure 1(d)) is obtained by peeling off the SU8 layer from the polystyrene surface after the SU8 layer is cross-linked and strong enough.

For method B, Part A and part B of smooth cast 305 are mixed together (10:9 by weight) and cast into a petri-dish to form a layer of pre-cure slab. After a pre-curing time, the rubber-like smooth cast slab is peeled off from the petri dish and attached onto the polystyrene nanocrack surface (Figure 1(c1)). Air bubbles trapped between the two slabs should be removed carefully. The two-slab system is sandwiched by a force measurement system (Model TSF, Mark-10®) with a given pressure applied for a certain period of time (pressurized time), as shown in Figure 1(c2). After releasing of the pressure,

the smooth cast slab on the polystyrene surface is left in air for a certain period of time until the smooth cast is solidified and strong enough for peeling off. Finally, a nanochannel mold can also be obtained by peeling off the smooth cast layer from the nanocrack surface (Figure 1(d)). All the nanocracks, nanochannel molds and nanochannels are observed and characterized by an optical microscope (Nikon, TE-2000) and an Atomic Force Microscope (AFM, Multimode™ SPM, Digital Instruments).

2.3 Bi-layer PDMS microchannel and nanochannel fabrication

PDMS is an excellent material for making microfluidic chips and can also be used to replicate nanofluidic chips. However, nanopatterns with a feather size smaller than 200 nm can hardly survive after bonding if they are made of regular PDMS due to the low Young's modulus (2~3 MPa) of the regular PDMS material [46]. To improve the Young's modulus of regular PDMS and to create stable patterns with a size smaller than 50 nm, extra hard PDMS (x-PDMS) [46] with Young's modulus as high as 80 MPa is employed in this work.

The following is the working processes for making x-PDMS. X-PDMS is composed of two parts, part A (vinyl functional part) and part B (cross linker part). An initial compound of Part A is prepared by mixing 10 g linear vinyl siloxanes (VDT 731) with 16 g Q-silocanes solution (VQX-221) and heating in an air-purged oven at 50℃ for 24 hours to evaporate the solvent. Afterwards, the final Part A is obtained by mixing 25μL platinum catalyst (SIP 6831.2LC) and 60 μL moderator (SIT 7900.0) into 1.8 g the mixture mentioned above. The pre-curing x-PDMS solution can be obtained by further mixing 0.6 g part B (linear silicon-hydride siloxane, HMS 501) into part A. All the chemicals used in the x-PDMS fabrication are purchased from Gelest Inc.

The pre-curing x-PDMS solution is degased in a vacuum oven (Isotemp® 280A) for 1~2 min and cast onto the nanochannel mold followed by a 30-minute-heating at 70℃ to solidify the x-PDMS (Figure 1(e)). The spin-coated x-PDMS layer is about 30~50μm thick. Then, another layer of regular PDMS of 3 mm thick is cast onto the x-PDMS layer (Figure 1(f)) followed by a second round of heating process at 80℃ for 2 hours. Finally, the bi-layer PDMS nanochannel is peeled off from the channel mold (Figure 1(g)).

The PDMS nanochannel will bridge a microchannel system to form the final nanofluidic chip. The microchannel chip contains a pair of "U" shaped microchannels designed by AutoCAD® software, and the microchannel mold is fabricated by the standard soft photolithography method. Figure 1(h) shows an example of the "U" shaped PDMS microchannel system. To avoid collapsing of the channel roofs during the chip bonding, the microchannel is also replicated by the bi-layer process as described above.

2.4 Chip bonding

Plasma bonding has been widely used to seal microfluidic or nanofluidic chips. X-PDMS has similar properties of regular PDMS and can be bonded together after plasma treatment. Before bonding, four channel wells are punched on the PDMS microchannel slab, and scotch tape is used to clean dusts or debris on the microchannel and nanochannel surfaces. Afterwards, the PDMS slabs are treated with plasma for 30 s (Harrick plasma®, PDC-32G) and bonded together by using a homemade alignment system (see the ESI† for the detail of the homemade alignment system). For all the processes, no clean room is needed.

3. Results and discussion

3.1 Fabrication of single nanocracks and nanocrack arrays

Controlling the locations of the nanocracks. Solvent-induced crack formation on polystyrene surfaces can be divided into three steps: crack initiation, crack propagation and crack termination [47]. In the first step, nanocracks start at defects or flaws on the surface; in the propagation step, nanocracks become larger, releasing surface stress; and in the termination step, no more stress can be released and the nanocracks stop

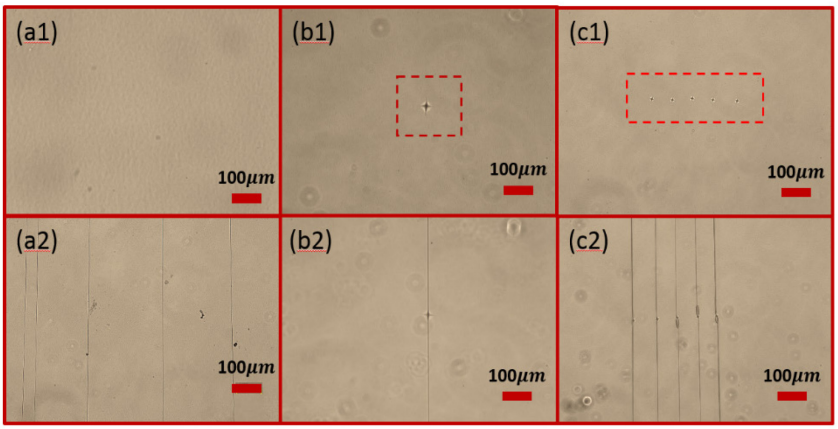

Figure 2 Examples of polystyrene surfaces before and after nanocrack generation under the same working condition of the solvent-induced method: (a1-a2) without artificial defects, (b1-b2) with one single artificial defect and (c1-c2) with multiple artificial defects.

growing. To initiate nanocracks, defects, such as sharp dents, flaws and molecular inhomogeneity, are needed to work as the stress nucleation sites. Therefore, artificial defects can be used to initialize nanocracks. Figure 2 shows examples of polystyrene surfaces before and after nanocrack generation by the solvent-induced method without artificial defects (Figure 2(a1-a2)), and with one single artificial defect (Figure 2(b1-b2)) as well as with multiple artificial defects (Figure 2(c1-c2)). It is obvious that the locations of the nanocracks generated on the polystyrene surface without artificial defects are random (Figure 2(a2)), and the artificial defects can control the locations of the single nanocrack and the nanocrack array precisely, as shown in Figure 2(b2) and Figure 2(c2).

Effects of the defect size on the number and size of nanocracks. To study the defect size effects on the creation of nanocracks, different forces ranging from 10 gF to 1000 gF were applied on the indenter to create defects on polystyrene surfaces. For each polystyrene sample surface, only one defect was created; and for each force value, 7 independent surface samples were prepared. For all the cases, the solvent-induced working parameters were the same: heating 1 mL 90% ethanol at 90℃ for 24h. Both the total number and the size of the nanocracks were recorded.

The results (see Figure 2S (a) and Figure 2S (b) of the ESI† for the detail) show that defects with larger sizes make the creation of nanocracks easier; however, more than one nanocrack may be generated on each larger defect (see Figure 2S (c)) due to higher stress concentration near the defect. On the other hand, using smaller artificial defects benefits creation of single nanocracks.

To obtain average crack size reliably, all the measurement locations are far away from the defects. The results show that the size of single nanocracks induced by single defects created with the same working condition have an essentially the same average size, about 140 nm wide and 28 nm deep (see the ESI†, Figure 3S (a)). As a result, the defects only dominate the initiation of the cracking and have little effect on the average size of the fully developed cracks.

However, artificial defects may affect the size of the crack at positions close to the defects. For example, the nanocrack sizes were measured at four points separated by 50μm along the nanocrack near a defect made by a force of 200 gF. The crack size is 338 nm in width and 68.8 nm in depth at the tip of the diamond-shaped defect, which is much larger than the average crack size, 140 wide and 28 nm deep, measured sufficiently far away from the defect. However, these values decrease to 147 nm wide and 34 nm deep at the point of 150 μm away from the tip of the defect, which is close to the average size of the cracks (see Figure 3S (b)of the ESI† for detail). While the artificial defects do affect the size of the induced nanocracks at positions close to the defect, however, this effect becomes negligible at points that are 150 μm away from the defects.

Smaller single nanocrack fabrication. Single nanocracks with a smaller size can also be generated by using artificial defects according to the guideline [45]. Figure 3 shows one of smaller single nanocracks generated on polystyrene surfaces by

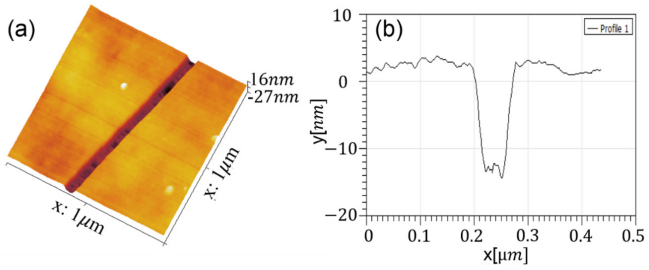

Figure 3 Nanocrack of 80 ±7.5nm wide and 16 ±5 nm deep generated on polystyrene surface by heating 0.8 mL 100% ethanol at 70℃ for 5.5 hours. (a) 3D image and (b) a cross section profile of the nanocrack measured by the AFM.

heating 0.8 mL 100% ethanol at 70℃ for 5.5 hours. The artificial defect was marked by a force of 10 gF. Figure 3(a) is a 3D view of the nanocrack and Figure 3(b) is the cross-section of this nanocrack of about 80 nm wide and 16 nm deep, as measured by the AFM.

3.2 Fabrication of nanochannel molds

3.2.1 Method A — UV curable soft lithography by using SU8 photoresist

Effects of photoresist type (solvent content). Six photoresists of SU8 2000 series were used to replicate nanocracks from polystyrene surfaces according to the working procedures in the previous part. More experimental details can be found in the ESI†.

Figure 4(a) shows the roughness of both the polystyrene cracks' sufaces and SU8 nanochannel mold surfaces after photoresist replication. From Figure 4(a) one can see that the surface roughness of both the crack surfaces and the photoresis channel molds increases with the concentration of

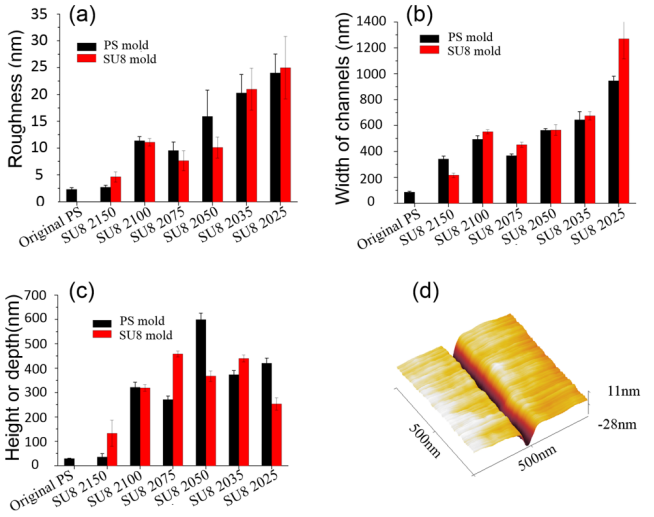

Figure 4 Nanochannel mold replication by using different types of SU8 photoresist. (a) Roughness of SU8 nanochannel mold surfaces and polystyrene (PS) crack surfaces after replication; (b) Width of SU8 nanochannel molds and polystyrene cracks after replication; (c) Height of SU8 nanochannel molds and depth of nanocracks on polystyrene after replication; (d) 3D image of the original nanocrack of 90 nm wide and 30 nm deep.

sovlents in the photoreists. For example, the roughness of the original polystyrene crack surface is about 2.5 nm, and this value increases to approximately 5 nm in the case of SU8 2150. For SU8 2025 with the highest concentration of solvents, the surface roughness reaches, approximately 25nm. Photoresists with higher concentration of sovents need longer time to evaporate after coating onto the polystyrene surface, and the solvents will swell polystyrene surfaces, which in turn results in higher level of surface roughnesses.

Figure 4(b) and Figure 4(c) show the size of the nanocracks and the replicated SU8 molds after the replciation process. It is obvious that the width of the nanocarcks and the SU8 nanochannel molds increases with the solvent concentraion, from about 200nm for the case of SU8 2150 to almost 1μm for the case of SU8 2025. The depth of the nanocracks and the height of the nanochannel molds also increase with the sovent concentation generally. As discussed above, to make nanochannel molds from the cracks on polystyrene surfaces with a smaller size changes and a smaller surface roughness, SU8 2150 is the optimal choice.

Effects of spin-coating time. The solvents in the SU8 photoresists affect not only the size of the nanochannel molds but also the size uniformity of the nanochannel molds. A lower viscosity of the photoresist contributes to a better fluidity and makes the filling of the photoresist into nanocracks easier. For the reason discussed above, to replicate nanocracks with a smaller size with lower surface roughness, SU8 2150 with lower concentration of solvents is essential. However, the viscosity of SU8 2150 photoresist is high, it is difficult to make SU8-2150 flow into the nanocracks in a short time; as a result, one has to control the SU8 2150 filling time effectively. After extensive experimental investigations, a spin-coating time of 120s is recommonded for using SU8 2150 photoresist (see the ESI† for the experimental details spin-coating time effect).

Effects of UV exposure dose. UV light can crosslink SU8 photoresist layers and make the nanochannel molds stable. In this part, SU8 2150 was used to study the effects of UV exposure dose on the nanochannel mold replication. The results show that for the underexposure cases, the photoresist layers are not fully cross-linked, and the photoresist layers are soft and sticky, one has to wait for several minutes before the photoresist molds are strong enough for peeling off. Therefore, the final channel mold surfaces are rough and the channel mold sizes are larger due to further swelling of the polystyrene surfaces (the nanocracks). In contrast, an overexposure of UV is able to minimize the swelling problems related to deforming of nanocracks, higher level of roughness of mold surfaces, or even failure of replication. However, overexposure UV energy will give rise to over cross-linked photoresist layers. As a result, the channel molds become brittle and very easy to break during the peeling off process. Based on the extensive experimental studies of this work (see the ESI† for the experimental details UV exposure dose effect), to make durable and intact nanochannel molds with a layer of 200μm thick SU8-2150 photoresist, the exposure UV energy should be larger than the standard exposure dose, around 800 mJ/cm^2.

Thickness of the photoresist layer. The thickness of SU8 photoresist layers also affects the size and the quality of the replicated nanochannel molds. To examine this effect, a series of photoresist layers from 80μm to 650μm obtained by spin-coating SU8 2150 at different spin coating speed ranging from 1000 rpm to 8000 rpm for 120 seconds onto polystyrene surfaces with nanocracks were used to fabricate the nanochannel molds. To minimize the time of solidification, all the samples were overexposed to UV light for 1200 mJ/cm^2 (see the ESI† for the details of the photoresist layer thickness effect).

The results (as shown in Figure 6S of the ESI†) show that the channel mold size decreases with the thickness of SU8 layer, because, on one hand, a thicker SU8 layer will generate more heat during the cross-linking process, which will reheat the nanocracks and trigger a larger crack size. On the other hand, a thicker layer of SU8 photoresist contains more solvents, which makes the time of evaporation longer; consequently, the solvents will further swell the polystyrene surface and give rise to a larger crack size. As a result, for SU8 2150 photoresist, a higher spin-coating speed (thinner photoresist layer) will improve the quality of the nanochannel mold.

3.2.2 Method B — Nanoimprint by smooth cast

Effects of smooth cast type. Three kinds of smooth cast, i.e., smooth cast 300, smooth cast 305 and TASK 4 were used to replicate nanocracks. Smooth cast 300 can cure in 10 minutes at room temperature and generate a large amount of heat, which will increase the size of the nanocracks significantly. It is also hard to control the replication process precisely due to the fast curing process. TASK 4 has a higher concentration of solvents and a lower viscosity. While TASK 4 can replicate the finest detail, the high concentration of solvents will further swell the polystyrene surfaces and make the unstable cracks much larger. Compared with Smooth cast 300 and TASK 4, smooth cast 305 has a moderate curing time and moderate solvents contents and is suitable for nanocrack replication.

To improve the fidelity of the nanoimprint technique by using Smooth cast 305, one needs to handle at least four parameters. The first one is the pre-curing time, which denotes the period of time from the mixing of part A and part B of smooth cast 305 to the start of nanocrack imprint. After the pre-curing time, the rubber-like smooth cast layer is attached onto a polystyrene surface with the nanocrack. The applied pressure and the pressurized time are critical parameters during the nanoimprint. The last parameter is the peeling off time, which is the time from the moment of mixing of part A and part B of smooth cast to the moment of peeling off of the smooth cast layer from the polystyrene surface. Peeling off time dominates the integrity of the nanochannel molds.

Pre-curing time. The pre-curing time affects the nanoimprint process in three aspects. Firstly, pre-curing time determines the fluidity of the smooth cast layer. The longer the pre-curing time, the harder the material will be, and a larger pressure has to be applied on the smooth cast material during the imprint in order to obtain the identical pattern of the nanocrack. Secondly, the pre-curing time controls the solvent content of

the smooth cast layer, which affects the swelling level of the polystyrene surface during replication. The longer the pre-curing time, the lower concentration of the solvent in the smooth cast layer and the lower swelling effects will be. Lastly, pre-curing time decides the temperature of the smooth cast layer. The heat generated in the smooth cast layer due to chemical reactions and crosslinking of molecules at the beginning of mixing will give more energy to the nanocracks and results in a larger size. As the pre-curing time becomes longer, the smooth cast will cool down, and the temperature effect is minimized.

Based on the large amount of tests conducted in this study (see the ESI† for the experimental details of the pre-curing time effects and the figures of the results), a recommended pre-curing time for smooth cast 305 is around 25~30 min, in room temperature ranging from 23 to 27℃. A higher room temperature will speed up the crosslinking process of smooth cast and give rise to a shorter pre-curing time.

Effects of pressure. Pressure is an important parameter for the nanoimprint. If the pressure is too high, the nanocracks on polystyrene surfaces are likely to deform or break up, and the crack sizes will become larger. On the other hand, if the pressure is too low, the smooth cast material may not flow into some parts of the nanocracks; consequently, the channel molds may be shallower than that of the original nanocracks, or even no nanochannel mold can be produced at all. To study the pressure effects, nanocracks with an average size of 300 nm in width and 60 nm in depth on polystyrene surfaces were replicated onto smooth cast layers with pressure values ranging from 0.25 MPa to 5 MPa. The experimental results (see the ESI† for the details of the experiments and Figure 8S for the results) show that the optimal pressure value for the nanoimprint by smooth cast 305 is around 0.5~1.5 MPa under the condition of 25 min pre-curing time.

Pressurized time. The pressurized time and the pressure are critical to the filling of smooth cast in the nanocracks during replication. Pressurized time from 5s to 10 min was studied. The original nanocracks are about 300 nm wide and 60 nm deep. In all the cases, the pre-curing time was 25 min, the pressure applied was 1 MPa, and the peeling off time was 60 min.

Experimental results show that the width of the channel molds has little change when the pressurized time increases from 5 s to 5 min. However, the depth of the channels increases with the increasing pressurized time, from about 20 nm to nearly 50 nm when the pressurized time increases from 40 s to 1 min. A longer pressurized time allows more smooth cast material flowing into the nanocracks. However, when the pressurized time is longer than 3 min, a higher chance of further cracking will take place. On the other hand, a pressurized time shorter than 15 s results in a higher degree of surface roughness and a lower success ratio of the replication. Examples of the pressurized time effects can be found in Figure 9S of the ESI†. A suitable pressurized time for smooth cast 305 should be around 1 min when the pre-curing time is 25 min and a pressure value of 1 MPa.

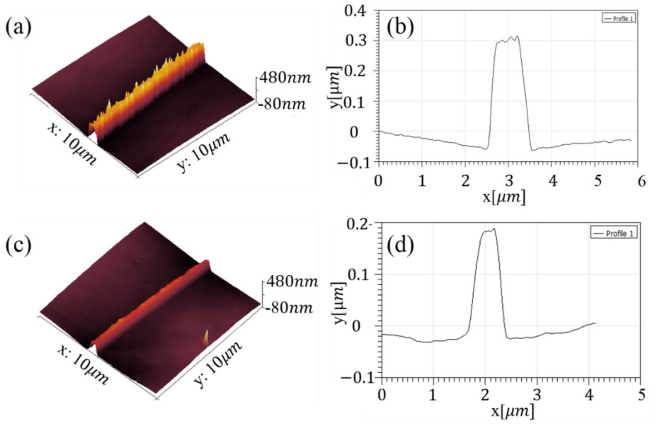

Figure 5 Comparison of positive nanochannel molds replicated by using smooth cast 305 and SU8 2150 from nanocracks with similar size, 570 nm in width and 160 nm in depth. (a) 3D image of the nanochannel mold replicated by SU8 2150, and (b) a cross section of the channel mold of 1021±31 nm in width and 362±18 nm in height. (c) 3D image of the nanochannel mold replicated by smooth cast 305, and (d) a cross section of the channel mold of about 616±15 nm in width and 232±9 nm in height.

Peeling off time. The peeling off time is also an important parameter for nanoimprint in smooth cast-polystyrene system. Peeling off earlier can minimize the contacting time between the smooth cast layers and the polystyrene with nanocracks. While a short contact time can reduce the swelling of the polystyrene surfaces, however, the smooth cast material squeezed in the cracks is still soft and sticky, consequently, the channel molds are likely to be deformed or broken during the peeling off process (see the ESI† for the details and exampls of the peeling off time effects). Based on the results of the extensive experimental investigation, a proper peeling off time is recommended as 60 min. Fine adjustment of the operation parameters can further improve the fidelity of the nanochannel molds to the original nanocracks. An example of fabrication of smooth cast nanochannel mold with highly uniform cross sections by using the optimal working parameters can be found in Figure 11S of the ESI†.

3.2.3 Comparison of method A and method B

Overall, both SU8 and smooth cast can be used to replicate nanocracks on polystyrene surfaces. Figure 5 compares positive nanochannel molds replicated by both smooth cast 305 and SU8 2150 from nanocracks with the similar size, about

Table 1 Summary and evaluation of SU8 method and Smooth cast method.

	SU8	Smooth cast
Optimal working parameters	Photoresist type: SU8 2150 Photoresist layer: 80μm @8000rpm Coating time: 120s UV exposure dose: ~800 mJ/cm^2	Smooth cast type: Smooth cast 305 Pre-curing time: 25~30 min Pressure: 1 MPa Pressurized time: 1~3 min Peeling off time: 60 min
Facilities	Spin-coater, UV exposure machine,	Micro-hardness testing system, pressure gauge, vacuum oven
Materials	SU 8 2150, PMMA slab	Smooth cast 305
Time cost	5~10 min	60~100 min
Price	Medium	Very low
Channel quality	Mold size generally is much larger than that of the original cracks. The roughness of the channel mold surfaces is about 5 nm.	Mold size generally is larger than that of the original cracks by 10% ~ 20%. Surface roughness is about 2~3 nm, similar to that of the original nanocrack surface.

570 nm in width and 160 nm in depth. Figure 5(a) is the nanochannel mold replicated by SU8 2150, the mold size is 1021±31nm in width and 362±18 nm in height. Figure 5(c) shows the nanochannel mold replicated by smooth cast, the mold size is 616±15 nm in width and 232±9 nm in height. One can see that the nanochannel mold replicated by smooth cast has a smaller size and a smoother surface compared with that replicated by SU8 2150 photoresist owing to the higher solvent concentration in the SU8 2150. A higher concentration of solvent will further swell and dissolve the nanocracks on the polystyrene surface and give rise to a larger replicated channel size. Table 1 summarizes the optimal working parameters for both methods and evaluates both methods by comparing the facilities, cost, durability, channel quality and so on. From Table 1 one can see that the major advantage of using SU8 is the significantly short processing time, and the disadvantage is that the mold size is much larger than the size of the original nanocrack. Using the smooth cast method, while the process takes much longer time, the mold size is generally more close to the size of the original nanocrack.

3.3 Fabrication of PDMS nanochannels

Durability of nanochannel molds. PDMS nanochannels can be made from these nanochannel molds by following the procedures of bi-layer PDMS nanochannel fabrication described in the previous section. Durable nanochannel molds are crucial for fabricating of sealed PDMS nanochannel chips with high repeatability. The durability of both SU8 photoresist nanochannel molds and smooth cast nanochannel molds were studied by duplicating bi-layer PDMS nanochannels from each mold for at least 6 times. Figure 6(a) shows the average sizes of PDMS nanochannels replicated from a single SU8 nanochannel mold for six times, and Figure 6(b) shows an 3D image of a PDMS nanochannel replicated from the SU8 nanochannel mold and a cross section profile of this channel. Clearly, all the channels are about 715 nm wide and 90 nm deep, with 1.5% and 11% deviation in the width and depth directions, respectively. Figure 6(c) shows that the sizes of PDMS channels replicated from one smooth cast nanochannel mold for 7 times; all these channels are about 220 nm wide and 40 nm deep, with 12% and 9.5% deviation in the width and depth directions, respectively. Figure 6(d) shows an AFM 3D image of the PDMS nanochannel replicated from the nanochannel mold duplicated by smooth cast and a cross section profile of this channel. In conclusion, both smooth cast nanochannel molds and SU8 photoresist nanochannel molds are sufficiently durable for replicating of PDMS nanochannels with little size change.

Fabrication of smaller PDMS nanochannels. As mentioned above, smooth cast works better in smaller naocrack replication. Figure 7 shows AFM images and profiles measured during a smaller PDMS nanochannel fabrication process by using a smooth cast nanochannel mold. Figure 7(a) is the original nanocrack on polystyrene surface with a size of approximately 95±10 nm in width and 35±4 nm in depth. Figure 7(b) is a positive nanochannel mold of smooth cast replicated from this nanocrack (a), and the mold size is

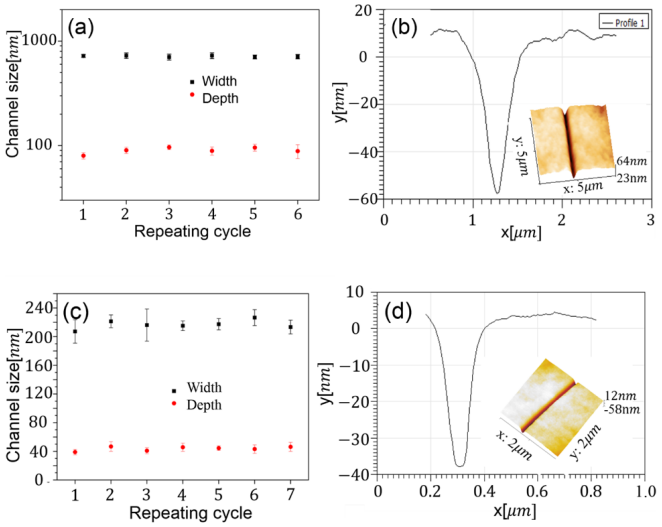

Figure 6 (a) Size of PDMS nanochannels replicated from one SU8 single nanochannel mold for 6 times. (b) 3D view of a PDMS nanochannel replicated from the nanochannel mold and a cross section profile of this nanochannel, about 715 nm wide and 90 nm deep.(c) Size of nanochannels replicated from one smooth cast channel mold for 7 times. (d) 3D view of a nanochannel replicated from nanochannel mold made of smooth cast and a cross section profile of this channel, about 220 nm wide and 40 nm deep.

104±12 nm in width and 43±5 nm in height. Figure 7(c) is the PDMS nanochannel replicated from this nanochannel mold (b); the nanochannel size is approximately 106±10 nm in width and 40±7nm in depth. The nanocrack on the polystyrene surface was formed by heating 1 mL 90% ethanol at 85℃ for 3.5 hours. The defect on the polystyrene was marked by the

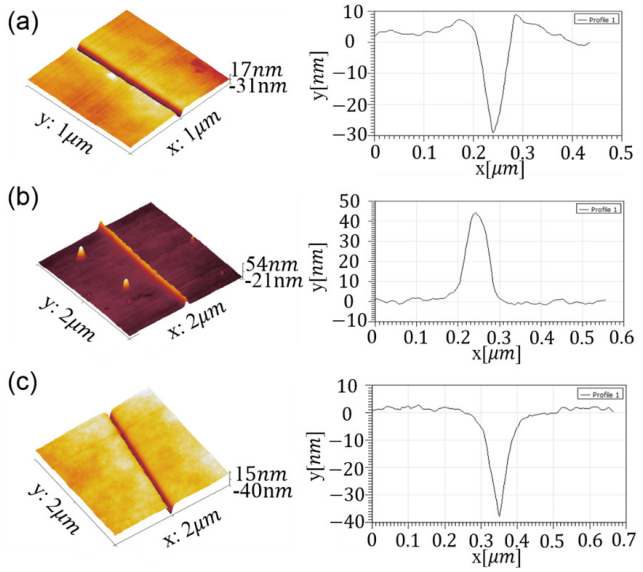

Figure 7 Replication of a nanochannel mold and a PDMS nanochannel from a nanocrack. (a) A negative nanocrack on polystyrene surface (95±10 nm wide and 35±4 nm deep), (b) A positive nanochannel mold on smooth cast (104±12 nm wide and 43±5 nm high) replicated from (a), (c) A negative nanochannel on PDMS (106±10 nm wide and 40±7 nm deep) replicated from the smooth cast channel mold (b).

indenter tip with a force of 50 gF. The smooth cast nanochannel mold was fabricated with the following operating parameters: a pre-curing time of 27 min and a pressure of 1 MPa with a pressurized time of 1 min, and a peeling off time of 60 min. The smooth cast method can produce even smaller nanochannels. An example of PDMS nanochannel of approximately 60 nm in width and 20 nm in depth replicated from a smooth cast nanochannel mold can be found in Figure 12S of the ESI†.

3.4 Chip bonding

X-PDMS has similar properties of regular PDMS, which can form sealed chips by plasma bonding. Bi-layer PDMS nanochannel slab and a bi-layer PDMS microchannel slab are placed in the plasma cleaner chamber and treated with plasma for 30 s. After the treatment, the surfaces can be bonded together by using the homemade alignment system (see the ESI†, Figure 1S). Figure 8 shows (a) a PDMS nanofluidic chip with single nanochannel after bonding and (b) a PDMS nanofluidic chip with parallel nanochannels after bonding. Figure 8(c) is an example of the final nanofluidic chip. Figure 8(d) shows a cross section of the bi-layer PDMS nanochannel after bonding and Figure 8(e) is a zoomed-in view of this nanochannel cross section measured by the AFM. To make sure these nanochannels are open after bonding, these nanochannels were tested by filling an electrolyte solution and applying an electric field and measuring the electric current. The results show that the nanochannels as small as 20 nm are still open after bonding.

3.5 Practical applications

Single nanochannel devices and multiple nanochannel devices have wide applications, such as manipulation of individual nanoparticles or molecules, stretching of DNA, biomolecular preconcentration and electrokinetic transport phenomena in nanoscale. To prove the reliablity of the PDMS nanochannel devices made by the methods developed in this paper, a series

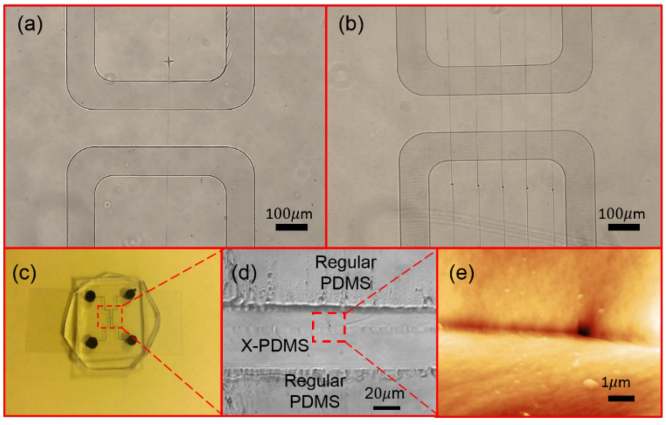

Figure 8 Nanofluidic chip after bonding. (a) PDMS nanofluidic chip with single nanochannel; (b) PDMS nanofluidic chip with parallel nanochannels, (c) An example of final PDMS nanofluidic chip, (d) Cross section of the bi-layer PDMS nanochannel, (e) Zoomed-in view of the cross section measured by the AFM.

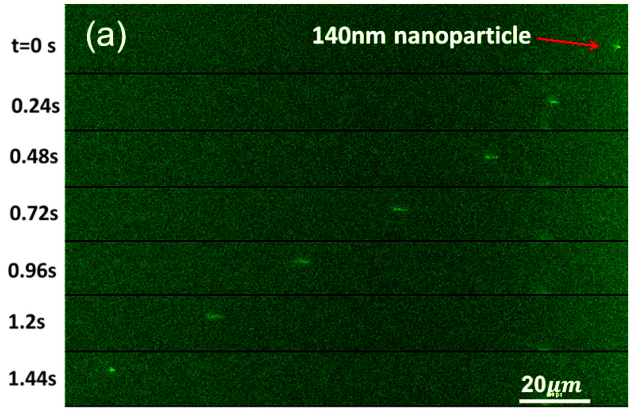

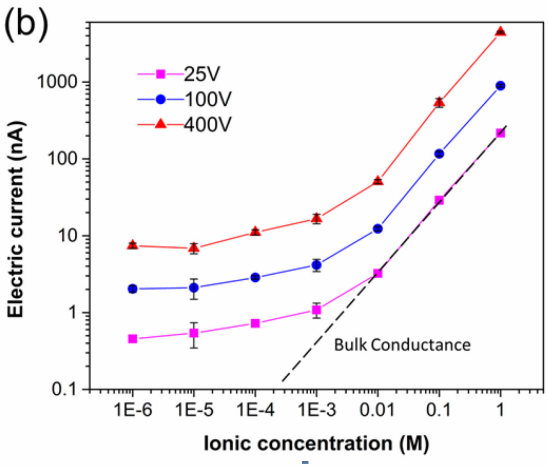

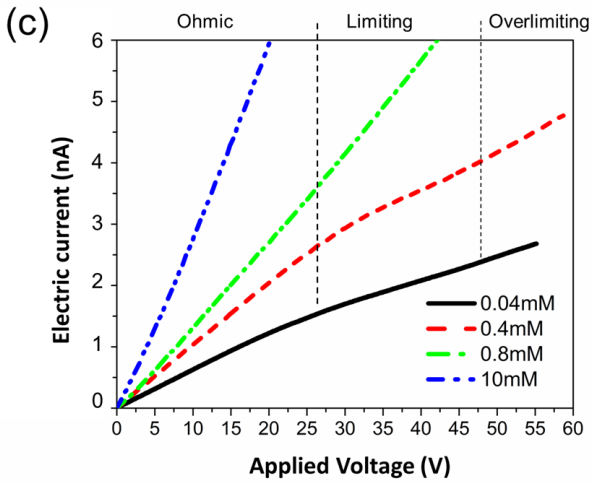

Figure 9 Practical examples of nanochannel devices. (a) Electrophoresis of a 140nm nanoparticle in a 340nm deep nanochannel; (b) surface-charge-governed ion transport in a single nanochannel of 254 nm deep; (c) ohmic-limiting-overlimiting current behavior in a single nanochannel of 174nm deep.

of parctical experiements have been conducted. For example, Figure 9(a) shows an example of electrophoretic motion of a 140nm fluorescent nanoparticle in a single nanochnnel of 340nm deep, 500nm wide and 300μm long with 20V/cm electric field applied. The nanoparticle is suspended in 10^{-4}M LiBr solution. The figures are captured by the fluorescent microscope (see the ESI† for the video). From the trajectory the average apparent velocity of this nanopaticle is around

$70\mu m/s$. Similarly, manupulation of single molecules can also be conducted in such devices. A systematical study of electroosmotic flow in PDMS nanochannels has also been investigated by our group[4]. To study the electical characteristics of the PDMS nanochannels, conductivity of PDMS nanochannels filled with electrolyte solutions with different ionic concentrations has been measured by electrometer (Keithley, 6517A). Figure 9(b) shows the concentration effects and the applied electric field effects on the electric current in a 254nm deep, 873nm wide and 200 μm long nanochannel filled with KCl solutions (see Figure 13S for the detail of the nanochannel). Obviously, the current increases with the concenration almost linearly when the concentration is higher than 10^{-2}M (the slope of the black dashed line depicts the conductance of the bulk solution). The conductivity of the nanochannel is strongly enhanced under the condition of low ionic strength compared with that of the bulk solutions with the same ionic strength due to the surface-charge-governed ion transport properties in nanochannels [48]. Similar experimetal results can be found elsewhere [49]. In addition, ohmic-limiting-overlimiting behavior [50,51] in nanochannels has also been studied. Figure 9(c) shows an example of I-V curves in a 174nm deep, 509nm wide and 200 μm long nanochannel filled with KCl solutions measured by the electrometer. DC power was applied between the nanochannel with an increment of 0.1V step for 3s duration through Pt electrodes. Clearly, when the applied electric field is lower than 25V, the currents are essentially linear with the aplied electric voltage; as the electric field increases, a limiting region appears for the low concentration cases (0.04mM and 0.4mM); however, as the electric field inceases further, the I-V curves become linear again, which is called the "overlimiting" region[50–52].

4. Conclusions

This article presents a novel method to fabricate PDMS nanofluidic chips with a single nanochannel or multiple nanochannels of controllable channel size and spacing. Long nanochannels of sub-100 nm in width and depth can be obtained by this method. In this method, artificial defects marked on polystyrene surface by hardness testing indenter are used to position the nanocracks created by the solvent-induced method. Nanocracks can be replicated onto either SU8 photoresist by soft lithography method or smooth cast by nanoimprint technique to produce nanochannel molds. X-PDMS supported by regular PDMS is used to replicate nanochannels from the channel molds to avoid collapsing of the channel roofs during device bonding. Micro-nanofluidic chips are obtained by bonding a PDMS nanochannel chip onto a PDMS microchannel chip. Based on the extensive experimental investigations, two sets of optimal working parameters for both the SU8 and the smooth cast methods are developed. The method described in this paper provides a powerful tool for fabricating disposable and inexpensive PDMS nanofluidic devices with single or multiple nanochannels with high reliability. Several practical examples by using these nanofluidic chips have also been demonstrated in this paper. The method of fabricating nanofluidic devices as developed in this work can be applied in almost every lab and will greatly facilitate the fundamental studies of transport phenomena in nanoscale and enable further development of nanofluidics based applications.

Acknowledgements

The authors wish to thank the financial support of the Natural Sciences and Engineering Research Council (NSERC) of Canada through a research grant to Dr. Li.

References

1 H. Daiguji, *Chem. Soc. Rev.*, 2010, **39**, 901–911.
2 A. Piruska, M. Gong, J. V Sweedler and P. W. Bohn, *Chem. Soc. Rev.*, 2010, **39**, 1060–72.
3 W. Sparreboom, a van den Berg and J. C. T. Eijkel, *Nat. Nanotechnol.*, 2009, **4**, 713–720.
4 R. Peng and D. Li, *Nanoscale*, 2016, 12237–12246.
5 P. Terejánszky, I. Makra, P. Fürjes and R. E. Gyurcsányi, *Anal. Chem.*, 2014, **86**, 4688–4697.
6 K. Zhou, L. Li, Z. Tan, A. Zlotnick and S. C. Jacobson, *J. Am. Chem. Soc.*, 2011, **133**, 1618–1621.
7 Z. D. Harms, K. B. Mogensen, P. S. Nunes, K. Zhou, B. W. Hildenbrand, I. Mitra, Z. Tan, A. Zlotnick, J. P. Kutter and S. C. Jacobson, *Anal. Chem.*, 2011, **83**, 9573–9578.
8 K. Aïzel, V. Agache, C. Pudda, F. Bottausci, C. Fraisseix, J. Bruniaux, F. Navarro and Y. Fouillet, *Lab Chip*, 2013, **13**, 4476–4485.
9 D. L. Yongxin Song, Hongpeng Zhang, Chan Hee Chon, Shu Chen, Xinxiang Pan, *Anal. Chim. Acta*, 2010, **681**, 82–86.
10 L. H. Thamdrup, A. Klukowska and A. Kristensen, *Nanotechnology*, 2008, **19**, 125301.
11 L. Guo, X. Cheng and C. Chou, *Nano Lett.*, 2004, **4**, 69–73.
12 C. H. Reccius, S. M. Stavis, J. T. Mannion, L. P. Walker and H. G. Craighead, *Biophys. J.*, 2008, **95**, 273–86.
13 L. D. Menard and J. M. Ramsey, *Anal. Chem.*, 2012, **85**, 1146–1153.
14 D. Huh, K. L. Mills, X. Zhu, M. A. Burns, M. D. Thouless and S. Takayama, *Nat. Mater.*, 2007, **6**, 424–428.
15 S. Li, J. Li, K. Wang, C. Wang, J. Xu, H. Chen, X. Xia, Q. Huo and U. States, *ACS Nano*, 2010, **4**, 6417–6424.
16 S. Chung, J. H. Lee, M.-W. Moon, J. Han and R. D. Kamm, *Adv. Mater.*, 2008, **20**, 3011–3016.
17 S. Yu, S. B. Lee, M. Kang, C. R. Martin, V. Uni and V. Gaines, *Nano Lett.*, 2001, **1**, 495–498.
18 M. Napoli, P. Atzberger and S. Pennathur, *Microfluid. Nanofluidics*, 2011, **10**, 69–80.
19 T. M. Wynne, A. H. Dixon and S. Pennathur, *Microfluid. Nanofluidics*, 2012, **12**, 411–421.
20 S. Tan, L. Wang, H. Liu, H. Wu and Q. Liu, *Nanoscale Res. Lett.*, 2016, **11**, 50.
21 C. Duan, W. Wang and Q. Xie, *Biomicrofluidics*, 2013, **7**, 26501.

22 Y. Chen, *Electrophoresis*, 2001, **22**, 187–207.
23 D. Mijatovic, J. C. T. Eijkel and A. van den Berg, *Lab Chip*, 2005, **5**, 492–500.
24 B. D. Gates, Q. Xu, M. Stewart, D. Ryan, C. G. Willson and G. M. Whitesides, *Chem. Rev.*, 2005, **105**, 1171–96.
25 T. Chen, I. Amin and R. Jordan, *Chem. Soc. Rev.*, 2012, **41**, 3280–96.
26 B. J. Lin, *J. Vac. Sci. Technol.*, 1975, **12**, 1317.
27 S. Hector, *Microelectron. Eng.*, 1998, **42**, 25–30.
28 R. Selzer and J. Heaton, *Microelectron. Eng.*, 2000, **53**, 591–594.
29 M. J. O'Brien, P. Bisong, L. K. Ista, E. M. Rabinovich, a. L. Garcia, S. S. Sibbett, G. P. Lopez and S. R. J. Brueck, *J. Vac. Sci. Technol. B Microelectron. Nanom. Struct.*, 2003, **21**, 2941.
30 S. Kim, B. Marelli, M. a Brenckle, A. N. Mitropoulos, E.-S. Gil, K. Tsioris, H. Tao, D. L. Kaplan and F. G. Omenetto, *Nat. Nanotechnol.*, 2014, **9**, 306–10.
31 A. a Tseng, *J. Micromechanics Microengineering*, 2004, **14**, R15–R34.
32 A. a Tseng, *Small*, 2005, **1**, 924–39.
33 K. S. Chu, S. Kim, H. Chung, J.-H. Oh, T.-Y. Seong, B. H. An, Y. K. Kim, J. H. Park, Y. R. Do and W. Kim, *Nanotechnology*, 2010, **21**, 425302.
34 W. Gong, J. Xue, Q. Zhuang, X. Wu and S. Xu, *Nanotechnology*, 2010, **21**, 195302.
35 L. Zhang, F. Gu, L. Tong and X. Yin, *Microfluid. Nanofluidics*, 2008, **5**, 727–732.
36 R. Fan, Y. Wu, D. Li, M. Yue, A. Majumdar and P. Yang, *J. Am. Chem. Soc.*, 2003, **125**, 5254–5.
37 A. Noy, H. Park and F. Fornasiero, *Nano Today*, 2007, **2**, 22–29.
38 S. Xu and Y. Zhao, *Microfluid. Nanofluidics*, 2011, **11**, 359–365.
39 S. Park and Y. Huh, *PNAS*, 2009, **106**, 15549–15554.
40 B. Kim, J. Heo, H. J. Kwon, S. J. Cho, J. Han, S. J. Kim and G. Lim, *ACS Nano*, 2013, **7**, 740–747.
41 D. Huh, K. L. Mills, X. Zhu, M. A. Burns, M. D. Thouless and S. Takayama, *Nat. Mater.*, 2007, **6**, 424–428.
42 N. Bowden, W. T. S. Huck, K. E. Paul and G. M. Whitesides, *Appl. Phys. Lett.*, 1999, **75**, 2557.
43 X. Zhu, K. L. Mills, P. R. Peters, J. H. Bahng, E. H. Liu, J. Shim, K. Naruse, M. E. Csete, M. D. Thouless and S. Takayama, *Nat. Mater.*, 2005, **4**, 403–6.
44 B.-Y. Xu, J.-J. Xu, X.-H. Xia and H.-Y. Chen, *Lab Chip*, 2010, **10**, 2894–901.
45 R. Peng and D. Li, *Biomicrofluidics*, 2015, **9**, 024117.
46 M. Verschuuren, Utrecht University, 2010.
47 O. Spurr and W. Niegisch, *J. Appl. Polym. Sci.*, 1962, **VI**, 585–599.
48 D. Stein, M. Kruithof and C. Dekker, *Phys. Rev. Lett.*, 2004, **93**, 035901.
49 C. Duan and A. Majumdar, *Nat. Nanotechnol.*, 2010, **5**, 848–852.
50 G. Yossifon, P. Mushenheim, Y.-C. Chang and H.-C. Chang, *Phys. Rev. E*, 2009, **79**, 046305.
51 S. J. Kim, Y. C. Wang, J. H. Lee, H. Jang and J. Han, *Phys. Rev. Lett.*, 2007, **99**, 1–4.
52 I. Cho, G. Y. Sung and S. J. Kim, *Nanoscale*, 2014, **6**, 4620–6.